

Article

Complexation Behavior of Pinene–Bipyridine Ligands towards Lanthanides: The Influence of the Carboxylic Arm

Atena B. Solea^{1,2}, Liangru Yang³, Aurelien Crochet², Katharina M. Fromm², Christophe Allemann¹
and Olimpia Mamula^{1,*}

¹ Haute Ecole d'Ingénierie et d'Architecture Fribourg, HEIA-FR, HES-SO, University of Applied Sciences of Western Switzerland, Pérolles 80, CH-1705 Fribourg, Switzerland; Atena.Solea@warwick.ac.uk (A.B.S.); Christophe.Allemann@hefr.ch (C.A.)

² Department of Chemistry, University of Fribourg, Chemin du Musée 9, CH-1700 Fribourg, Switzerland; aurelien.crochet@unifr.ch (A.C.); katharina.fromm@unifr.ch (K.M.F.)

³ School of Chemistry & Chemical Engineering, Henan University of Technology, Zhengzhou 450001, China; lryang@haut.edu.cn

* Correspondence: olimpia.mamulasteiner@hefr.ch

Abstract: The complexation behavior of two novel, chiral pinene–bipyridine-type ligands ((–)-HL1 and (–)-HL2) containing a carboxylic arm towards lanthanide Ln(III) (Ln = La, Eu, Lu) ions was investigated through spectroscopic methods. The association constants of the mononuclear complexes determined from the UV-Vis titrations indicated that the ligand (–)-HL1 possessing a shorter carboxylic arm formed more stable complexes compared with (–)-HL2, whose carboxylic arm had one more methylene unit. This is due to the formation of more stable seven-member metal chelate rings in the first case as compared with the eight-member metal chelate rings in the second. IR and fluorescence spectroscopy provided additional information about the structure of these complexes.

Keywords: pinene–bipyridine ligands; lanthanide complexes; association constants; UV-Vis spectroscopy; self-assembly; supramolecular chemistry; solution equilibria



Citation: Solea, A.B.; Yang, L.; Crochet, A.; Fromm, K.M.; Allemann, C.; Mamula, O. Complexation Behavior of Pinene–Bipyridine Ligands towards Lanthanides: The Influence of the Carboxylic Arm. *Chemistry* **2022**, *4*, 18–30. <https://doi.org/10.3390/chemistry4010002>

Academic Editor: Edwin Charles Constable

Received: 8 December 2021

Accepted: 27 December 2021

Published: 31 December 2021

Publisher's Note: MDPI stays neutral with regard to jurisdictional claims in published maps and institutional affiliations.



Copyright: © 2021 by the authors. Licensee MDPI, Basel, Switzerland. This article is an open access article distributed under the terms and conditions of the Creative Commons Attribution (CC BY) license (<https://creativecommons.org/licenses/by/4.0/>).

1. Introduction

The use of coordination chemistry for the development of large, discrete, supramolecular architectures by self-assembly is well known. The strength of the interaction and the directionality induced by the coordination bonds can be more effective in self-assembly processes than just H-bonding or van der Waals forces [1]. Indeed, a plethora of discrete, supramolecular architectures based on coordination bonds (e.g., coordination cages [2–5], or helicates [6]) have been obtained.

Often, the complexity of the self-assembled species increases with the coordination number of the metal ions. Such a behavior can be expected for the lanthanide ions Ln(III) due to their large ionic radii and high coordination numbers. Moreover, their interesting features such as large Stokes shifts, emission [7], and magnetic properties [8] can lead to the formation of self-assembled architectures with interesting functionalities [9]. Such Ln(III) complexes have found many applications in lanthanide–actinide extraction processes [10,11], bioimaging [12], sensing [13], lighting and displays [14–18], or as single-molecular magnets [8,19]. However, the lability and the lack of directionality typical for the dative bonds formed by Ln(III) ions render the diastereoselective synthesis of enantiopure, self-assembled polynuclear structures quite challenging. To date, only a few ligands, such as the ones shown in Figure 1, have been reported to successfully control the structure and to induce the chirality of the resulting architectures. With the introduction of two stereogenic centers on ligand E1, the complexation of Eu(III) leads to the formation of a mixture of a helicate and a tetrahedral cage [20]. Similarly, a heptameric, homochiral Eu(III) wheel could be obtained both directly or stepwise, by using the chiral ligand, E2 [21].

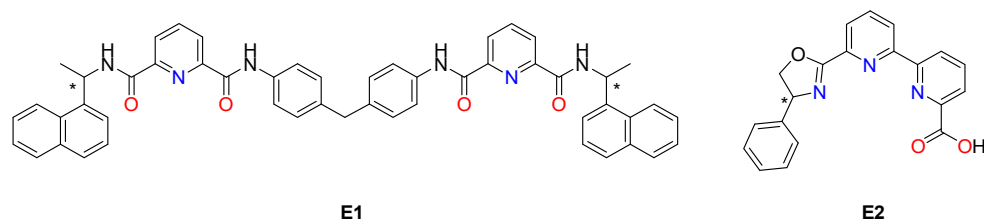


Figure 1. Examples of chiral ligands used for the diastereoselective self-assembly of polynuclear lanthanide complexes.

Previously, our group succeeded to functionalize the (–)-5,6-pinene bipyridine ligand by a diastereoselective introduction of a carboxylic arm into the pinene moiety. The ligand obtained, (+)-HL0, was successfully used as a chiral building block for the self-assembly of enantiopure, trinuclear helicates with Eu(III) [22,23]. This complex also showed a solvent-dependent trinuclear-tetranuclear interconversion [24]. In the trinuclear compound $[\text{Ln}_3(\text{L0})_6(\mu_3\text{-OH})(\text{H}_2\text{O})_3]^{2+}$ there are two sets of ligands, each showing a different coordination mode. Three ligands are bidentate and connect two adjacent metal centers by coordinating solely via their carboxylate group. They form 5-membered chelate cycles. The other three are tetradentate and besides the carboxylate they are coordinating as well with their two nitrogens from the bipyridine unit leading to 6-membered chelate cycles (Figure 2a).

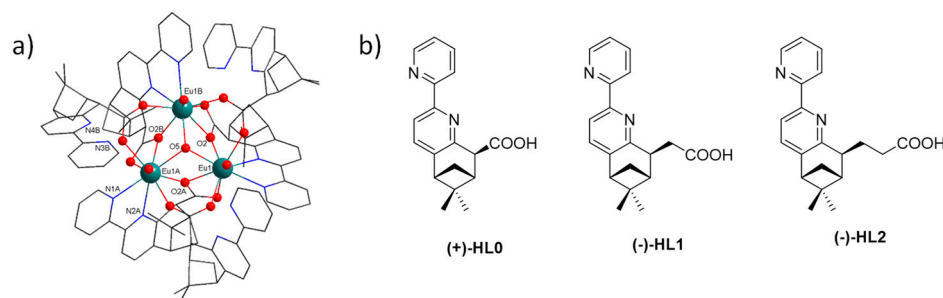


Figure 2. (a) Structure of the trinuclear complex formed by (+)-HL0 with Eu(III) ions as determined by single-crystal X-ray diffraction [23]. (b) The structure of the three analogue ligands.

To understand the influence of the ligand design on the self-assembly process and the stability of the obtained architectures, we decided to modify the ligand (+)-HL0 by increasing the length of the carboxylic pendant arm. Thus, we synthesized the new ligands (–)-HL1 (one more CH_2 unit) and (–)-HL2 (two more CH_2 units) (Figure 2b). Here, we report the results of our study about the influence of the pendant arm length on the coordination behavior with various Ln(III) ions.

2. Materials and Methods

2.1. General

Reagent grade chemical, including the anhydrous solvents, were purchased from Sigma Aldrich and Acros Organics and used without further purification. $\text{Eu}(\text{ClO}_4)_3 \cdot n\text{H}_2\text{O}$ and $\text{Lu}(\text{ClO}_4)_3 \cdot n\text{H}_2\text{O}$ were synthesized as previously reported [25]. *Caution! Perchlorate salts are potentially explosive.* The amount of water in $\text{Ln}(\text{ClO}_4)_3 \cdot n\text{H}_2\text{O}$ ($n = 7.6$ for $\text{Ln} = \text{La}$, $n = 6.3$ for $\text{Ln} = \text{Eu}$, $n = 5.6$ for $\text{Ln} = \text{Lu}$) was determined by Karl–Fischer titrations on a Mettler Toledo C10s coulometric Karl–Fischer titrator. Yields reported are for isolated, spectroscopically pure compounds. When inert conditions were required, the reactions were performed under the Ar atmosphere using glassware dried overnight at 120 °C. Analytical thin layer chromatography (TLC) was performed on SiO_2 plates GF254 (0.25-mm layer thickness). Flash chromatography purifications were performed on a CombiFlash EZ Prep from Teledyne®. Optical rotations were measured on an Anton Paar Modular Circular

Polarimeter MCP 100. The measurements were carried out in a quartz vessel ($l = 100$ mm) with the sodium D line of a sodium lamp (589 nm) using spectroscopic-grade solvents. IR spectra were recorded as solids between $4000\text{--}400$ cm^{-1} on a Bruker ALPHA FTIR. UV-Vis spectra were recorded at 20 °C on an Evolution 220 spectrometer from Thermo Scientific equipped with a thermostat. Fluorescence spectra were recorded at 20 °C on a Fluoromax 4 spectrometer from HORIBA equipped with a thermostat. NMR spectra were recorded on a Bruker Advance DPX 300 spectrometer using TMS or the residual solvent proton as internal standard. HRMS spectra were recorded on FTMS 4.7T BioAPEX II and Waters SynaptG2-Si. ESI-MS spectra were recorded on a Thermo Trace DSQ II and Voyager GC-MS. Crystallographic data were collected on a STOE IPDS-II diffractometer.

2.2. General Procedure for (–)-PL

Under inert atmosphere, freshly distilled diisopropylamine (DIA) (5.25 mL, 37.1 mmol) was dissolved in 210 mL of anhydrous THF. The solution was cooled to -20 °C. BuLi (38 mmol 17.5 mL, 2.2 M in hexane) was added. The reaction mixture was heated at 0 °C and left stirring for 10 minutes. Afterwards the mixture was cooled to -40 °C and a solution of (–)-5,6-pinene bipyridine (7 g, 28 mmol) in anhydrous THF (105 mL) was added dropwise for 30 minutes. The solution instantly turned dark blue. The reaction mixture was then stirred for 2 h at -40 °C. After this time, ally bromide (1.5 equiv., 5.08 g, 3.6 mL, 42 mmol) (for (–)-PL1) or 4-bromo-1-butene (1.5 equiv., 5.67 g, 4.3 mL, 42 mmol) (for (–)-PL2) was added and the mixture was stirred at -40 °C for 1 h and then allowed to reach RT. Gradually, the mixture turned dark green and afterwards light brown. The mixture was stirred for 16 h. Afterwards, the remaining base was quenched with 2.1 mL H_2O and the solvent was removed under rotary evaporation. The compound was purified by column chromatography on silica 60, eluent: hexane/EtOAc = 4/1.

(–)-PL1: Rf = 0.6. Yield: 76%. ^1H NMR (300 MHz, CDCl_3) δ 8.64 (ddd, $J = 4.8, 1.8, 0.9$ Hz, 1H, H1), 8.44 (dt, $J = 8.0, 1.1$ Hz, 1H, H4), 8.08 (dd, $J = 7.8, 0.7$ Hz, 1H, H7), 7.80 (ddd, $J = 8.0, 7.5, 1.8$ Hz, 1H, H3), 7.31 (d, $J = 7.8$ Hz, 1H, H8), 7.29–7.22 (m, 1H, H2), 5.97 (ddt, $J = 16.7, 10.2, 6.5$ Hz, 1H, H20), 5.12 (ddt, $J = 17.1, 2.2, 1.5$ Hz, 1H, H21a), 5.01 (ddt, $J = 10.2, 2.3, 1.2$ Hz, 1H, H21b), 3.09 (dt, $J = 10.0, 3.3$ Hz, 1H, H11), 2.80 (t, $J = 5.7$ Hz, 1H, H14), 2.62–2.53 (m, 1H, H13a), 2.52–2.42 (m, 1H, H12), 2.37–2.27 (m, 2H, H12, H19), 1.72–1.53 (m, 2H, H18), 1.44 (s, 3H, H17), 1.34 (d, $J = 9.8$ Hz, 1H, H13b), 0.65 (s, 3H, H16). ^{13}C NMR (75 MHz, CDCl_3) δ 159.60, 156.89, 153.19, 148.97, 142.12, 139.13, 136.77, 133.54, 123.03, 120.83, 117.75, 114.45, 46.92, 43.74, 43.46, 41.20, 32.07, 31.82, 28.54, 26.45, 20.94. HRMS (ESI) calcd. for $\text{C}_{20}\text{H}_{23}\text{N}_2^+$ $[\text{M} + \text{H}]^+$ 291.1861, found 291.1904. $[\alpha]_D^{20}$ (0.250 g/L in CH_2Cl_2): -115° .

(–)-PL2: Rf = 0.6. Yield: 83%. ^1H NMR (300 MHz, CDCl_3) δ 8.64 (ddd, $J = 4.8, 1.8, 0.9$ Hz, 1H, H1), 8.44 (dt, $J = 8.0, 1.1$ Hz, 1H, H4), 8.08 (dd, $J = 7.8, 0.8$ Hz, 1H, H7), 7.88–7.70 (m, 1H, H3), 7.31 (d, $J = 7.8$ Hz, 1H, H8), 7.28–7.22 (m, 1H, H2), 5.97 (ddt, $J = 16.8, 10.2, 6.5$ Hz, 1H, H20), 5.17–5.08 (m, 1H, H21a), 5.01 (ddt, $J = 10.2, 2.3, 1.2$ Hz, 1H, H21b), 3.09 (dt, $J = 10.0, 3.3$ Hz, 1H, H11), 2.80 (t, $J = 5.7$ Hz, 1H, H14), 2.64–2.52 (m, 1H, H13a), 2.52–2.39 (m, 1H, H12), 2.39–2.26 (m, 3H, H19), 1.69–1.52 (m, 2H, H18), 1.44 (s, 3H, H17), 1.34 (d, $J = 9.8$ Hz, 1H, H13b), 0.65 (s, 3H, H16). ^{13}C NMR (75 MHz, CDCl_3) δ 159.61, 156.89, 153.19, 148.97, 142.12, 139.13, 136.77, 133.54, 123.03, 120.83, 117.75, 114.45, 46.92, 43.74, 43.46, 41.20, 32.07, 31.82, 28.54, 26.45, 20.94. HRMS (ESI) calcd. for $\text{C}_{21}\text{H}_{25}\text{N}_2^+$ $[\text{M} + \text{H}]^+$ 305.20122, found 305.20091. $[\alpha]_D^{20}$ (0.100 g/L in CH_2Cl_2): -130° .

2.3. General Procedure for (–)-HL

Over (–)-PL (1.72 mmol) a mixture of acetone (17 mL), water (6 mL) and CH_3COOH (8 mL) was added. The suspension was cooled to 0 °C and solid KMnO_4 (5 equiv., 17.22 mmol, 2.721 g) was added in 5 portions over a period of 4 h at this temperature. The mixture was brought to RT and stirred for one more hour. After this time, a H_2O_2 35% solution was added dropwise until the complete dissolution of the precipitate. The obtained solution was extracted with CH_2Cl_2 (3×30 mL). The organic phase was washed with

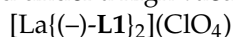
brine and dried over anhydrous MgSO_4 . The solvent was evaporated, and the crude product was purified by column chromatography on silica gel 60, eluent: $\text{CH}_2\text{Cl}_2/\text{MeOH} = 5/0.1$.

(-)-HL1: Obtained: 0.46 g light yellow oil. Yield: 43%. ^1H NMR (300 MHz, CDCl_3) δ 8.69 (ddd, $J = 4.8, 1.8, 0.9$ Hz, 1H, H1), 8.23–8.14 (m, 1H, H4), 8.06 (d, $J = 7.8$ Hz, 1H, H7), 7.82 (td, $J = 7.8, 1.8$ Hz, 1H, H3), 7.42 (dd, $J = 7.9, 1.2$ Hz, 1H, H8), 7.30 (ddt, $J = 6.9, 4.9, 1.0$ Hz, 1H, H2), 3.25 (dd, $J = 9.0, 6.6$ Hz, 1H, H11), 2.93 (ddd, $J = 14.6, 10.0, 7.6$ Hz, 1H, H19a), 2.84 (t, $J = 5.7$ Hz, 1H, H14), 2.75–2.66 (m, 1H, H19b), 2.66–2.56 (m, 1H, H13a), 2.25 (td, $J = 6.0, 2.5$ Hz, 2H, H18a, H12), 2.00 (ddd, $J = 16.9, 13.9, 7.0$ Hz, 1H, H18b), 1.44 (s, 3H, H17), 1.38 (d, $J = 10.0$ Hz, 1H, H13b), 0.64 (s, 3H, H16). ^{13}C NMR (75 MHz, CDCl_3) δ 176.89, 158.35, 155.60, 152.85, 149.31, 143.03, 137.27, 134.77, 123.50, 120.98, 119.15, 46.96, 45.47, 42.06, 41.71, 33.63, 29.25, 28.92, 26.20, 20.90. HRMS (ESI) calcd. for $\text{C}_{19}\text{H}_{21}\text{N}_2\text{O}_2^+$ $[\text{M}+\text{H}]^+$ 309.13975, found 309.15939. $[\alpha]_D^{20}$ (0.552 g/L in CH_2Cl_2): -109° .

(-)-HL2: Yield: 40%. ^1H NMR (300 MHz, CDCl_3) δ 8.69 (ddd, $J = 4.8, 1.8, 0.9$ Hz, 1H, H1), 8.23–8.14 (m, 1H, H4), 8.06 (d, $J = 7.8$ Hz, 1H, H7), 7.82 (td, $J = 7.8, 1.8$ Hz, 1H, H3), 7.42 (dd, $J = 7.9, 1.2$ Hz, 1H, H8), 7.30 (ddt, $J = 6.9, 4.9, 1.0$ Hz, 1H, H2), 3.25 (dd, $J = 9.0, 6.6$ Hz, 1H, H11), 2.93 (ddd, $J = 14.6, 10.0, 7.6$ Hz, 1H, H19a), 2.84 (t, $J = 5.7$ Hz, 1H, H14), 2.75–2.66 (m, 1H, H19b), 2.66–2.56 (m, 1H, H13a), 2.25 (td, $J = 6.0, 2.5$ Hz, 1H, H18a), 2.00 (ddd, $J = 16.9, 13.9, 7.0$ Hz, 1H, H18b), 1.44 (s, 3H, H17), 1.38 (d, $J = 10.0$ Hz, 1H, H13b), 0.64 (s, 3H, H16). ^{13}C NMR (75 MHz, CDCl_3) δ 177.01, 158.47, 155.72, 152.97, 149.43, 143.15, 137.40, 134.89, 123.62, 121.11, 119.27, 47.09, 45.60, 42.19, 41.84, 33.77, 29.39, 29.05, 26.34, 21.03. HRMS (ESI) calcd. for $\text{C}_{20}\text{H}_{23}\text{N}_2\text{O}_2^+$ $[\text{M} + \text{H}]^+$ 323.1760, found 323.1773. $[\alpha]_D^{20}$ (0.552 g/L in CH_2Cl_2): -140° .

2.4. General Procedure for the Synthesis of $[\text{LnL}_2](\text{ClO}_4)$

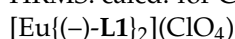
A solution of (-)-HL (0.08 mmol, 1 equiv.) in MeOH (0.35 mL) was treated with *N,N*-diisopropylethylamine (DIPEA, 14 μL , 0.08 mmol, 1 equiv.) and stirred for 5 min at RT. A saturated solution of $\text{Ln}(\text{ClO}_4)_3 \cdot n\text{H}_2\text{O}$ (0.04 mmol, 0.5 equiv.) in MeOH (0.2 mL) was added in one portion, and 2 mL *i*-Pr₂O were added to the reaction mixture and a white precipitate formed instantly. This was filtered, washed with a cold mixture of MeOH/*i*-Pr₂O (1:1), and dried under a high vacuum.



IR (cm^{-1}): 3112w ($\nu_{\text{O-H}}$), 2930w ($\nu_{\text{C-H}}$), 1556s ($\nu_{\text{as COO}^-}$), 1428s ($\nu_{\text{s COO}^-}$), 1057s ($\nu_{\text{Cl-O}}$), 621s ($\nu_{\text{Cl-O}}$).

(+)-ESI-MS: m/z (%) 309 (100) $[(+)\text{-HL1}+\text{H}]^+$, 639.9 (23) $[2(+)\text{-HL1}+\text{Na}]^+$, 752.8 (7) $[\text{La}\{(-)\text{-L1}\}_2]^+$.

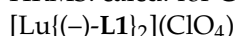
HRMS: calcd. for $\text{C}_{38}\text{H}_{38}\text{N}_4\text{O}_4\text{La}^+$ $[\text{La}\{(-)\text{-L1}\}_2]^+$ 753.1745, found 753.1742.



IR (cm^{-1}): 3107w ($\nu_{\text{O-H}}$), 2913w ($\nu_{\text{C-H}}$), 1556s ($\nu_{\text{as COO}^-}$), 1428s ($\nu_{\text{s COO}^-}$), 1045s ($\nu_{\text{Cl-O}}$), 621s ($\nu_{\text{Cl-O}}$).

(+)-ESI-MS: m/z (%) 309 (100) $[(+)\text{-HL1}+\text{H}]^+$, 766.8 (60) $[\text{Eu}\{(-)\text{-L1}\}_2]^+$.

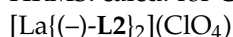
HRMS: calcd. for $\text{C}_{38}\text{H}_{38}\text{N}_4\text{O}_4\text{Eu}^+$ $[\text{Eu}\{(-)\text{-L1}\}_2]^+$ 765.1841, found 765.1180.



IR (cm^{-1}): 3111w ($\nu_{\text{O-H}}$), 2918w ($\nu_{\text{C-H}}$), 1557s ($\nu_{\text{as COO}^-}$), 1428s ($\nu_{\text{s COO}^-}$), 1093s ($\nu_{\text{Cl-O}}$), 621s ($\nu_{\text{Cl-O}}$).

(+)-ESI-MS m/z (%) 309 (100) $[(+)\text{-HL1}+\text{H}]^+$, 638.8 (45) $[2(+)\text{-HL1}+\text{Na}]^+$, 788.8 (20) $[\text{Lu}\{(-)\text{-L1}\}_2]^+$.

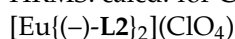
HRMS: calcd. for $\text{C}_{38}\text{H}_{38}\text{N}_4\text{O}_4\text{Lu}^+$ $[\text{Lu}\{(-)\text{-L1}\}_2]^+$ 789.2301, found 789.2283.



IR (cm^{-1}): 2930w ($\nu_{\text{C-H}}$), 1575s ($\nu_{\text{as COO}^-}$), 1430s ($\nu_{\text{s COO}^-}$), 1090s ($\nu_{\text{Cl-O}}$), 621s ($\nu_{\text{Cl-O}}$).

(+)-ESI-MS: m/z (%) 323.2 (100) $[(+)\text{-HL2}+\text{H}]^+$, 781.1 (5) $[\text{La}\{(-)\text{-L2}\}_2]^+$.

HRMS: calcd. for $\text{C}_{40}\text{H}_{42}\text{N}_4\text{O}_4\text{La}^+$ $[\text{La}\{(-)\text{-L2}\}_2]^+$ 781.2270, found 781.2242.



IR (cm^{-1}): 3112w ($\nu_{\text{O-H}}$), 2930w ($\nu_{\text{C-H}}$), 1555s ($\nu_{\text{as COO}^-}$), 1426s ($\nu_{\text{s COO}^-}$), 1096s ($\nu_{\text{Cl-O}}$), 621s ($\nu_{\text{Cl-O}}$).

(+)-ESI-MS m/z (%) 323 (100) [(-)-HL2+H]⁺, 794.9 (70) [Eu{(-)-L2}2]⁺.

HRMS: calcd. for C₄₀H₄₂N₄O₄Eu⁺ [Eu{(-)-L2}2]⁺ 793.2193, found 793.2206.

[Lu{(-)-L2}2](ClO₄)

IR (cm⁻¹): 3112w (ν_{O-H}), 2930w (ν_{C-H}), 1579s (ν_{as COO⁻}), 1429s (ν_{s COO⁻}), 1096s (ν_{Cl-O}), 621s (ν_{Cl-O}).

(+)-ESI-MS: m/z (%) 323 (10) [(-)-L2+H]⁺, 816.9 (100) [Lu{(-)-L2}2]⁺.

HRMS: calcd. for C₄₀H₄₂N₄O₄Lu⁺ [Lu{(-)-L2}2]⁺ 817.2593, found 817.2614.

2.5. UV-Vis Titrations

Stock solutions of ~0.2 mM [(-)-L] [(DIPEA)H] were prepared in anhydrous MeCN (100 mL) by dissolution of [(-)-L] [(DIPEA)H] (0.02 mmol: 8.68 mg [(-)-L1] [(DIPEA)H] and 9.03 mg [(-)-L2] [(DIPEA)H]), which were previously prepared by reaction between (-)-HL and DIPEA in DCM. These solutions were afterwards diluted with anhydrous MeCN to reach a final concentration of ~0.2 mM. The exact concentration of [(-)-L] [(DIPEA)H] was determined by UV-Vis spectrophotometry. Stock solutions of Ln(ClO₄)₃·*n*H₂O were prepared in anhydrous MeCN by quantitative dissolution of the salts at a concentration of ~10 mM, followed by dilution until a concentration of ~1 mM. The exact concentration of Ln(III) was determined afterwards by ICP-OES, then 2 mL of ~0.2 mM [(-)-L] [(DIPEA)H] solutions were titrated with microvolumes of Ln(III) solutions into UV-Vis cells with a path length of 1 cm, at 20 °C. Each titration was carried out in triplicate and the fitting was done on each titration. The results were averaged to give the final association constants.

2.6. ¹H NMR Titrations

Stock solutions of [(-)-L] [(DIPEA)H] of 0.167 M concentration were prepared by dissolution in MeOD; 1 M solutions of La(ClO₄)₃·7.6H₂O were prepared by dissolution of the salt in MeOD; 1 mL of [(-)-L] [(DIPEA)H] solutions were titrated with microliters of La(III) solutions into an NMR tube.

2.7. X-Ray Structure Determinations

Single crystals of (-)-PL1, (-)-HL2 were selected and mounted on loop with oil on a STOE IPDS II diffractometer. Crystals were kept at 250(2) K during data collection. A single crystal of (-)-HL1 was selected and mounted on loop with oil on a STOE STADIVARI diffractometer. Crystals were kept at 200(2) K during data collection. Using Olex2 [25], structures were solved with the SHELXT [26] structure solution program using intrinsic phasing and refined with the SHELXL [27] refinement package using least squares minimization.

Crystal data for:

(-)-HL1 C₁₉H₂₀N₂O₂ (*M* = 308.37 g/mol): orthorhombic, space group *P*2₁2₁2₁ (no. 19), *a* = 6.50130(10) Å, *b* = 10.1527(3) Å, *c* = 24.2770(5) Å, *V* = 1602.42(6) Å³, *Z* = 4, *T* = 200(2) K, μ(Cu Kα) = 0.668 mm⁻¹, *D*_{calc} = 1.278 g/cm³, 16497 reflections measured (14.102° ≤ 2θ ≤ 137.64°), 2908 unique (*R*_{int} = 0.0181, *R*_{sigma} = 0.0125) which were used in all calculations. The final *R*₁ was 0.0317 (*I* > 2σ(*I*)) and *wR*₂ was 0.0805 (all data).

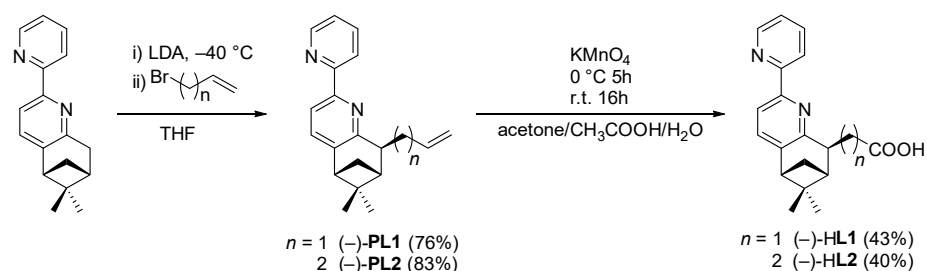
(-)-HL2: C₄₀H₄₄N₄O₄ (*M* = 644.79 g/mol): monoclinic, space group *P*2₁ (no. 4), *a* = 11.3097(8) Å, *b* = 6.2574(5) Å, *c* = 24.2538(19) Å, β = 95.828(6)°, *V* = 1707.6(2) Å³, *Z* = 2, *T* = 250(2) K, μ(MoKα) = 0.082 mm⁻¹, *D*_{calc} = 1.254 g/cm³, 5874 reflections measured (3.376° ≤ 2θ ≤ 50.516°), 5874 unique (*R*_{int} = MERG, *R*_{sigma} = 0.0900) which were used in all calculations. The final *R*₁ was 0.0896 (*I* > 2σ(*I*)) and *wR*₂ was 0.2532 (all data). Twinned data refinement scales 0.732(6):0.268(6).

(-)-PL1: C₂₀H₂₂N₂ (*M* = 290.39 g/mol): orthorhombic, space group *P*2₁2₁2₁ (no. 19), *a* = 7.2613(5) Å, *b* = 9.0056(6) Å, *c* = 25.277(2) Å, *V* = 1652.9(2) Å³, *Z* = 4, *T* = 250(2) K, μ(MoKα) = 0.068 mm⁻¹, *D*_{calc} = 1.167 g/cm³, 21498 reflections measured (3.222° ≤ 2θ ≤ 50.25°), 2947 unique (*R*_{int} = 0.1080, *R*_{sigma} = 0.0646) which were used in all calculations. The final *R*₁ was 0.0400 (*I* > 2σ(*I*)) and *wR*₂ was 0.0850 (all data).

3. Results and Discussion

3.1. Synthesis

The ligands (–)-HL1 and (–)-HL2 were obtained by introducing a pendant arm end-functionalized with a carboxylic acid moiety to (–)-5,6-pinene bipyridine [28]. The first step involved the diastereoselective deprotonation of the pinene unit by the bulky base LDA at $-40\text{ }^{\circ}\text{C}$, followed by nucleophilic attack on brominated allylic derivatives, leading to the formation of (–)-PL1 and (–)-PL2 in 76%, respectively, 83% yield (Scheme 1). In the second step, these allylic derivatives were oxidized in the presence of KMnO_4 , leading to the ligands (–)-HL1 and (–)-HL2, in 43%, respectively 40% yields. The formation of (–)-PL1, (–)-PL2, (–)-HL1, and (–)-HL2 was confirmed in solution by ^1H NMR, ^{13}C NMR, and HRMS.



Scheme 1. Synthetic procedure for the synthesis of ligands (–)-HL1 and (–)-HL2.

The structures of (–)-PL1, (–)-HL1, and (–)-HL2 were also confirmed in the solid state by single crystal X-ray diffraction.

The structure of (–)-PL1 (Figure 3) confirms the diastereoselective attachment of the pendant arm with the C13 atom in the *S* configuration, in agreement with previously reported similar reactions on the pinene unit [29]. The compound crystallizes in the $P2_12_12_1$ (no. 19) chiral space group, with one molecule in the asymmetric unit.

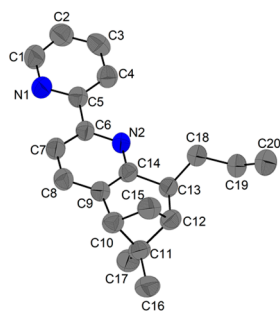


Figure 3. Molecular structure of (–)-PL1 determined by single-crystal X-ray diffraction with ellipsoids at 50% probability. The H atoms were omitted for clarity.

The compound (–)-HL1 (Figure 4, left) crystallizes in the $P2_12_12_1$ (no. 19) space group, with one molecule in the asymmetric unit. Intermolecular H-bonds involving the H of the carboxylic group of one molecule and the pyridine nitrogen N1 of the neighbouring one ($\text{O2-H2}\cdots\text{N1}$) are present. The strength of this interaction, as indicated by the O2-H2-N1 angle (168°) and the $\text{H2}\cdots\text{N1}$ distance (1.87 \AA), seems rather moderate [30]. The two pyridine rings form an angle of 15° between each other. Unlike the structures presented before, the compound (–)-HL2 possesses two molecules in the asymmetric unit. Similarly to (–)-HL1, each molecule is interacting with a neighboring one through moderate-strength H-bonding, as indicated by the $\text{H2A}\cdots\text{N1}$ and $\text{H4A}\cdots\text{N3}$ distances ($1.90(2)$, respectively $1.91(2)\text{ \AA}$) and the O2-H2A-N1 and O4-H4A-N3 angles ($160(2)^\circ$) [30]. The angles between the two planes described by the two pyridine rings are 9.3° for the first molecule (depicted) and 10.6° for the second molecule of the asymmetric unit. As in the case of (–)-PL1 and (–)-HL1, the structure of (–)-HL2 does not show any π - π or $\text{C-H}\cdots\pi$ interactions.

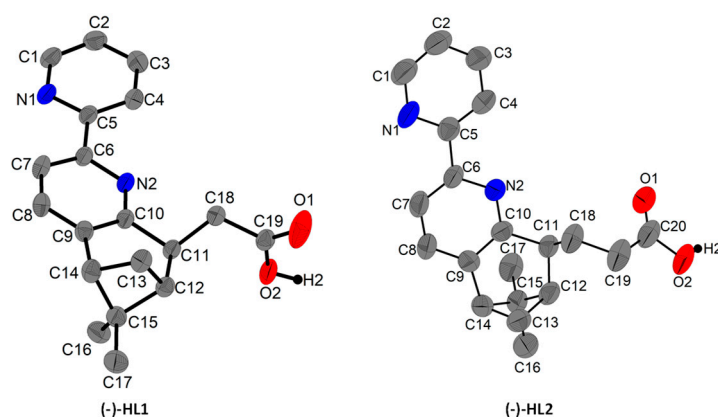


Figure 4. Molecular structure of (–)-HL1 (left) and one of the molecules in the asymmetric unit of (–)-HL2 (right), determined by single-crystal X-ray diffraction with ellipsoids at 50% probability. The H atoms were omitted for clarity.

3.2. Complexation Studies

(–)-HL1 and (–)-HL2 were employed as ligands for the synthesis of Ln(III) complexes by using the diamagnetic cations La(III) and Lu(III), and the intermediate-sized, but paramagnetic ion, Eu(III).

Previous studies with the ligand (+)-HL0, showed the formation of chiral supramolecular complexes in 1:2 or 1:3 metal-to-ligand ratios (M:L)[31]. Therefore, these two ratios were also used in the present study. The complexation reactions were carried out in the presence of 2 equiv. of a non-coordinating base, the *N,N*-diisopropylethylamine (DIPEA), by mixing concentrated methanolic solutions of deprotonated ligand with methanolic solutions of Ln(ClO₄)₃·*n*H₂O salts. The La(III), Eu(III), Lu(III) complexes were isolated by precipitation with diisopropyl ether. The complexes were analyzed by ESI-MS spectrometry, IR, and ¹H NMR spectroscopy.

The ESI-MS and IR spectra of the complexes formed with 1:2 and 1:3 M:L ratios, respectively, showed no significant difference, suggesting the formation of similar species in these conditions. In the ESI-MS spectra (see Supplementary Materials) recorded in MeOH, only the peak corresponding to [Ln{(–)-L1}₂]⁺ or [Ln{(–)-L2}₂]⁺ was found. No multinuclear species were detected as was the case of the complexes obtained with (+)-HL0 [22,23,32].

Further, the IR spectra of the amorphous powders were almost superimposable, suggesting isostructurality. Moreover, all showed strong bands at 1086 and 621 cm^{–1}, which stemmed from the stretching vibrations of the uncoordinated perchlorate ion [33]. Another specific feature of the spectra was the presence of a band centered at around 3112 cm^{–1}, which was indicative of O–H stretching. In addition, the two strong bands at 1580 and 1430 cm^{–1} stemmed from the two vibrational modes of the carboxylate moiety. According to the literature data [34–37], the coordination mode of the carboxylate unit can be determined from the difference $\Delta\nu = \nu_{as} - \nu_s$ of the carboxylate ion. In all the complexes isolated with both ligands, the difference $\Delta\nu$ was 150 cm^{–1}. This difference suggests a bidentate–cyclic coordination.

The ¹H NMR spectra of the compounds [LaL₂](ClO₄) (L = (–)-L1[–], (–)-L2[–]) in MeOD, CD₂Cl₂, and CDCl₃ showed broad signals at RT and also at higher (323 K) or lower temperature (233 and 183 K), indicating fluxionality or possible isomerization (Supplementary Materials, Figures S13–S16).

The Eu(III) complexes were also characterized by emission spectroscopy in CH₂Cl₂ (λ_{ex} = 270 nm, Figure 5). The typical narrow transition bands characteristic for Eu(III) complexes dominate both spectra and an efficient antenna effect from the ligands is observed. The presence of an antenna effect further suggests an efficient energy transfer from the ligands towards the metal center, thus indicating a coordination from at least one N atom from the bipyridine moieties. Moreover, the fine structure of the emission bands of both complexes can provide further information regarding the Eu(III) environ-

ment ion and its symmetry [15]. While the $^5D_0 \rightarrow ^7F_1$ transition is independent of the ligand field, the $^5D_0 \rightarrow ^7F_2$ transition is not, and is particularly influenced by the symmetry around the Eu(III) cation. A decreased symmetry around the metal ion center led to the increase of the $^5D_0 \rightarrow ^7F_2$ band intensity and thus the $^7F_2/{}^7F_1$ intensity ratio could be used to evaluate the coordination environment. Indeed, according to the literature [37], a ratio below 1 was observed for a centrosymmetric environment, while for asymmetric systems, the ratio is typically comprised between 8 and 12. In our case, the ratios are 3.0 for $[\text{Eu}(-)\text{-L1}]_2\text{ClO}_4$ and 4.8 for $[\text{Eu}(-)\text{-L2}]_2\text{ClO}_4$, indicating in both cases an asymmetric coordination environment around the Eu(III) ion.

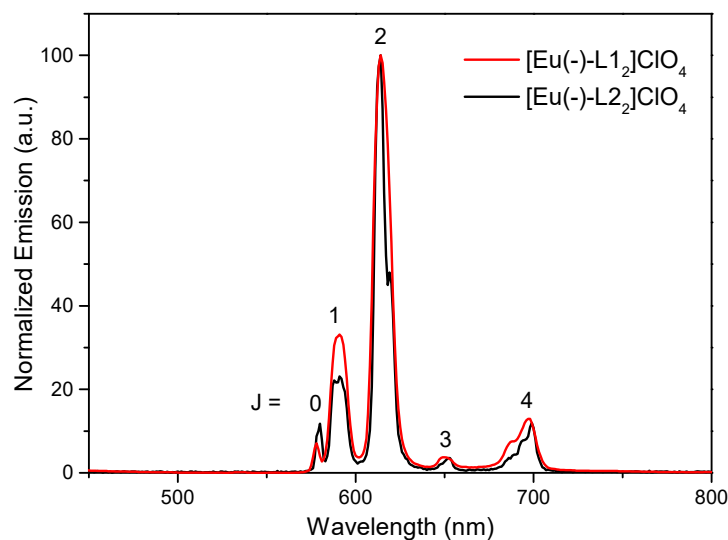


Figure 5. Normalized emission spectra of $[\text{Eu}(-)\text{-L}_2]_2\text{ClO}_4$ in CH_2Cl_2 (0.02 mM, $\lambda_{\text{ex}} = 270$ nm).

3.3. Determination of Association Constants by UV-Vis Titrations

Further, the association constants of the Ln(III) complexes (Ln = La, Eu, Lu) with the ligands $(-)\text{-L1}^-$ and $(-)\text{-L2}^-$ were determined by UV-Vis titrations in MeCN. For this, solutions of the deprotonated ligands (~ 0.02 mM) were titrated with increments of the corresponding Ln(III) solutions in MeCN (~ 1 mM). Due to the weak coordinating nature of the perchlorate ion, as confirmed by IR, perchlorate lanthanide salts were employed for the titrations ($\text{Ln}(\text{ClO}_4)_3 \cdot n\text{H}_2\text{O}$). Previous studies [38] have shown that the trans–cis isomerization (Figure 6) of the ligands can be followed through UV-Vis.

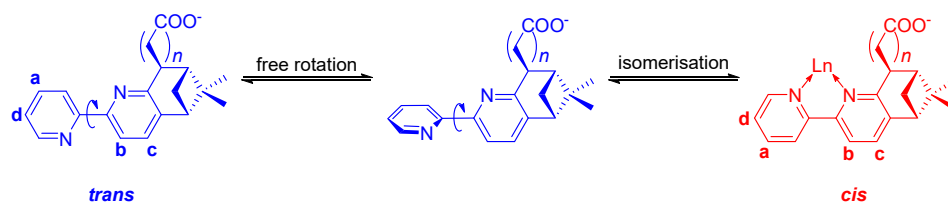


Figure 6. Isomerization of the bipyridine unit upon complexation.

When the ligand is in its free, uncoordinated form, the maximum of absorption is situated at 290 nm. The addition of coordinating metal ions induces a bathochromic shift to 315 nm, which is characteristic for the cis conformation of the bipyridine unit. The evolution of the UV-Vis spectra of the two ligands can be observed in Figure 7.

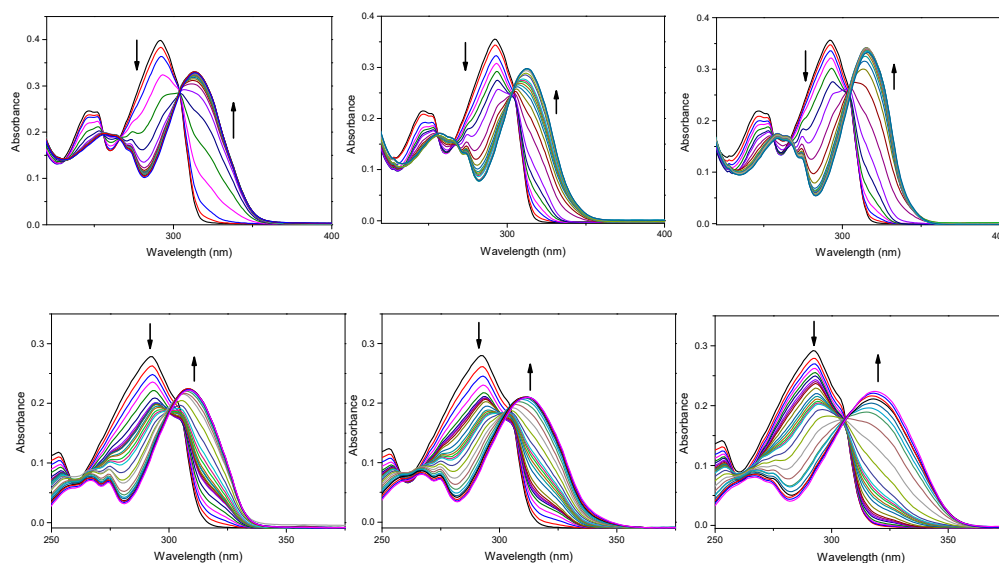
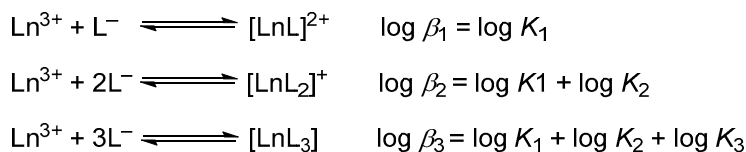


Figure 7. UV-Vis spectra of (–)-L1[−] in MeCN upon additions of La(III) (left), Eu(III) (middle), and Lu(III) (right) from 0 to 5 equivalents (top) and UV-Vis spectra of (–)-L2[−] in MeCN upon additions of La(III) (left), Eu(III) (middle), and Lu(III) (right) from 0 to 7 equivalents (bottom).

A global analysis of the spectra was further performed using the open-source titration Fitter [39] software. For the model, only mononuclear species were considered, as shown below:



The association constants obtained after the numerical fit of the curves are presented in Table 1. The values for the association constants obtained for both (–)-L1[−] and (–)-L2[−] were comparable along the series, following for each stoichiometry the expected trend (La³⁺ < Eu³⁺ < Lu³⁺) that reflects the continuous contraction of the ionic radius of lanthanides with increasing atomic number, the concomitant increase in charge density, and thus, the stronger electrostatic metal-ligand interaction. In addition, for both ligands and for any of the three cations, there was a slight decrease in binding constants moving from the species [LnL]²⁺ towards [LnL₃] (i.e., K₁ > K₂ > K₃), in agreement with the steady decrease of (i) the electrical positive charge of the metal species reacting with L[−], (ii) the number free coordination sites around the lanthanide cation, as expressed by the statistical factors [37], and (iii) the possible steric hindrance from the pinene units. The association constants found for ligand (–)-L1[−] are much stronger compared with those obtained with the ligand (–)-L2[−]. This reflects the major influence of the size of the chelate ring on the stability of the complexes. In the complexes with (+)-L0[−], the chelate cycles containing the N from the pinene bipyridine moiety and an O from the carboxylic unit have 6 atoms, while for the (–)-L1[−] and (–)-L2[−], 7- and 8-membered rings are formed, respectively. Thus, an increase of the length of the pendant arm disfavours complexation. Other tridentate bipyridine ligands containing the carboxylate ion and forming 5-atom chelate rings, such as those reported by Ziessel and coworkers [40], show cumulative association constants of 5.8(1), 10.6(1), and 14.6, respectively, lower than those obtained with (–)-L1[−], but similar to the ones obtained for (–)-L2[−]. They also observed higher differences in association constants along the lanthanide series, which is not the case with (–)-L1[−] and (–)-L2[−]. A thorough comparison is however difficult because the solvent used in both studies are different (water vs. acetonitrile). However, a big chelate cycle is not the only culprit for diminishing the association constants. In the case of an octadentate, bis-phosphonated bipyridine ligand,

very high association constants of around 19 were determined for the La(III), Eu(III), and Lu(III) mononuclear complexes, with no trend in association constant along the lanthanide series [41]. The ability of this ligand to enclose the lanthanide ion and shield it from the influence of water molecules is probably the source of the high association constants.

Table 1. Association constants in MeCN of the complexes formed with (–)-L1[–] and (–)-L2[–].

L	Ln	log K ₁	log K ₂	log K ₃	log β ₁	log β ₂	log β ₃
(–)-L1 [–]	La	7.9	6.3	5.6	7.9 ± 0.2	14.2 ± 0.4	19.8 ± 0.4
	Eu	8.0	6.4	5.1	8.0 ± 0.2	14.4 ± 0.1	19.5 ± 0.2
	Lu	8.7	6.4	5.0	8.7 ± 0.1	15.1 ± 0.1	20.1 ± 0.3
(–)-L2 [–]	La	5.1	4.6	5.3	5.1 ± 0.2	9.7 ± 0.2	15.0 ± 0.4
	Eu	5.1	4.7	5.4	5.1 ± 0.1	9.8 ± 0.1	15.2 ± 0.1
	Lu	4.9	4.9	5.7	4.9 ± 0.2	9.8 ± 0.3	15.5 ± 0.1

The influence of the size of the chelate ring was further evidenced by the concentration profiles of the formed species (Figure 8). They showed striking differences for the two ligands. In the case of (–)-L2[–], even in the presence of 2.5 equiv. of La(III) ions, free ligands as well as much lower concentrations of [La{(–)-L2}₂]⁺ and [La{(–)-L2}₃] species were observed.

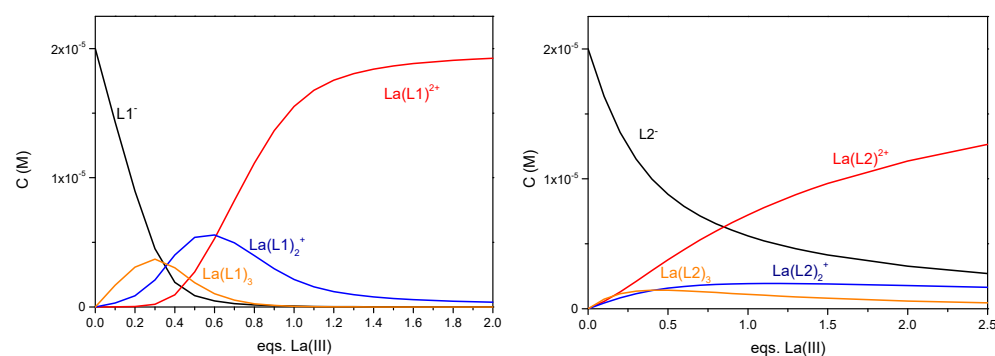


Figure 8. Concentration profiles of the species formed during the titrations of (–)-L1[–] (left) and (–)-L2[–] (right) with La(ClO₄)₃ in MeCN ([L[–]]_{Tot} = 0.02 mM).

3.4. ¹H NMR Titrations

¹H NMR titrations were also carried out on the deprotonated ligands (*c*~150 mM). Due to jellification in MeCN, the solvent employed was MeOD. La(ClO₄)₃·*n*H₂O was used as a model for the entire series, due to its similar behavior compared to the other Ln(III) ions observed in the UV-Vis titrations, as well as its diamagnetism.

Previous studies [38] have shown that the trans-cis isomerization of the 5,6-pyridine bipyridine can be monitored by ¹H NMR. Indeed, the addition of 1 equiv. of acid will isomerize the trans-bpy to its cis form, as the proton is shared between the two N atoms. The addition of 2 equiv. of acid will revert it back to the trans form, with both N atoms being protonated. In our case, the aim of these titrations was to identify the isomerization and the coordination modes of the ligands.

As can be seen in Figures S3 and S4, with increasing increments of La(III), both the aliphatic and aromatic peaks were shifted, but to a different extent. As both (–)-L1[–] and (–)-L2[–] have a pendant arm which contains the hard base COO[–], a good binding group for hard metal ions such as Ln(III), the shifts in the aliphatic regions indicate that this moiety is also involved in complexation. The chemical shifts for the aromatic signal **a** (Figure 6, Figures S3 and S4) were similar in both cases, indicating the same coordination behavior for both ligands. Firstly, the signal was shielded, reaching a maximum upfield shift Δδ at 0.3 equiv. La(III), while after this point the trend changed and the peak underwent a downfield shift, which, according to the previous studies [38], is indicative of the isomerization.

As expected, the aromatic protons (**b,c**) from the pyridine ring annealed to pinene show negligible shifts. Based on these findings and corroborating with the previously obtained UV-Vis data, we proposed the following binding behavior: First, the ligand binds via the COO^- group, while the bipyridine unit is still in its trans form, inducing an upfield shift in the unbound trans bipyridine. Afterwards, the bipyridine is starting to bind to La(III), isomerizing from trans to cis, as shown by the downfield of the aromatic protons starting from 0.5 equiv. La(III). The complete isomerization trans to cis is observed at a Ln:L ratio of 1:1.

4. Conclusions

The complexation behavior of two novel chiral ligands, $(-)\text{-L1}^-$ and $(-)\text{-L2}^-$, with Ln(III) ions was studied by UV-Vis, emission, and NMR spectroscopy in solution. The formation of three species in equilibrium, namely $[\text{LnL}]^{2+}$, $[\text{LnL}_2]^+$, and $[\text{LnL}_3]$, was demonstrated. By direct synthesis, species of the type $[\text{LnL}_2](\text{ClO}_4)$ were isolated, as shown by ESI-MS spectrometry and confirmed in the solid state by FT-IR. This behavior is completely different from what it was observed with the parent ligand $(+)\text{-L0}^-$, which forms discrete, trinuclear species in these conditions. The main explanation is given by the dimensions of the chelate rings, which possess decreasing stabilities in the order: 6 atoms (for $(+)\text{-L0}^-$) > 7 atoms (for $(-)\text{-L1}^-$) > 8 atoms (for $(-)\text{-L2}^-$). Indeed, the association constants confirm that increasing the chelate cycle to 7 atoms (L1^-) or to 8 atoms (L2^-) leads to less stable complexes. This study clearly demonstrates how relatively small structural modifications of the ligand can fundamentally change the output of the self-assembly processes.

Supplementary Materials: The following are available online at <https://www.mdpi.com/article/10.3390/chemistry4010002/s1>. Figure S1: Superposition of IR spectra of complexes with $(-)\text{-L1}^-$; Figure S2: Superposition of IR spectra of complexes with $(-)\text{-L2}^-$; Figure S3: ^1H NMR titration of $(-)\text{-L1}^-$ with La(III) in MeOD; Figure S4: ^1H NMR titration of $(-)\text{-L2}^-$ with La(III) in MeOD, NMR spectra, (+)-ESI-MS spectra, HRMS spectra. Figure S5: ^1H -NMR spectrum of $(-)\text{-PL1}$; Figure S6: ^{13}C -NMR spectrum of $(-)\text{-PL1}$; Figure S7: ^1H -NMR spectrum of $(-)\text{-HL1}$; Figure S8: ^{13}C -NMR spectrum of $(-)\text{-HL1}$; Figure S9: ^1H -NMR spectrum of $(-)\text{-PL2}$; Figure S10: ^{13}C -NMR spectrum of $(-)\text{-PL2}$; Figure S11: ^1H -NMR spectrum of $(-)\text{-HL2}$; Figure S12: ^{13}C -NMR spectrum of $(-)\text{-HL2}$; Figure S13: Stacked ^1H -NMR spectra of $[\text{La}\{(-)\text{-L2}\}_2]\text{ClO}_4$ in CD_2Cl_2 at 298 K (top), 233 K (middle) and 183 K (bottom); Figure S14: Stacked ^1H -NMR spectra of $[\text{La}\{(-)\text{-L1}\}_2]\text{ClO}_4$ in MeOD; Figure S15: ^1H -NMR spectrum of $[\text{Eu}\{(-)\text{-L1}\}_2]\text{ClO}_4$ in CDCl_3 ; Figure S16: ^1H -NMR spectrum of $[\text{Lu}\{(-)\text{-L1}\}_2]\text{ClO}_4$ in CDCl_3 .

Author Contributions: Conceptualization, O.M. and A.B.S.; methodology, A.B.S. and L.Y.; formal analysis, A.B.S.; investigation, A.B.S., A.C. and L.Y.; resources, O.M., C.A. and K.M.F.; writing—original draft preparation, A.B.S. and O.M.; writing—review and editing, A.B.S., O.M. and C.A.; supervision, O.M. All authors have read and agreed to the published version of the manuscript.

Funding: This research was funded by HES-SO research funds.

Acknowledgments: The authors wish to thank Albert Ruggi and Fredy Nydegger from University of Fribourg for the HRMS spectra, Felix Fehr for recording the VT ^1H NMR spectra and Frédéric Dux for assistance with the *titrationFitter* software.

Conflicts of Interest: The authors declare no conflict of interest.

References

1. Varshey, D.B.; Sander, J.R.G.; Frišćić, T.; MacGillivray, L.R. *Supramolecular Interactions*. In *Supramolecular Chemistry*; Gale, P.A., Steed, J.W., Eds.; Wiley: Hoboken, NJ, USA, 2012.
2. Kilbas, B.; Mirtschin, S.; Riis-Johannessen, T.; Scopelliti, R.; Severin, K. Dicarboxylate-bridged ruthenium complexes as building blocks for molecular nanostructures. *Inorg. Chem.* **2012**, *51*, 5795–5804. [[CrossRef](#)]
3. Jansze, S.M.; Cecot, G.; Wise, M.D.; Zhurov, K.O.; Ronson, T.K.; Castilla, A.M.; Finelli, A.; Pattison, P.; Solari, E.; Scopelliti, R.; et al. Ligand Aspect Ratio as a Decisive Factor for the Self-Assembly of Coordination Cages. *J. Am. Chem. Soc.* **2016**, *138*, 2046–2054. [[CrossRef](#)] [[PubMed](#)]

4. Zarra, S.; Wood, D.M.; Roberts, D.A.; Nitschke, J.R. Molecular containers in complex chemical systems. *Chem. Soc. Rev.* **2015**, *44*, 419–432. [[CrossRef](#)]
5. Metherell, A.J.; Ward, M.D. Stepwise synthesis of a Ru₄Cd₄ coordination cage using inert and labile subcomponents: Introduction of redox activity at specific sites. *Chem. Commun.* **2014**, *50*, 6330–6332. [[CrossRef](#)] [[PubMed](#)]
6. Von Zelewsky, A.; Mamula, O. The bright future of stereoselective synthesis of co-ordination compounds. *J. Chem. Soc. Dalton Trans.* **2000**, 219–231. [[CrossRef](#)]
7. Bünzli, J.C.G.; Piguet, C. Taking advantage of luminescent lanthanide ions. *Chem. Soc. Rev.* **2005**, *34*, 1048–1077. [[CrossRef](#)] [[PubMed](#)]
8. Woodruff, D.N.; Winpenny, R.E.P.; Layfield, R.A. Lanthanide Single-Molecule Magnets. *Chem. Rev.* **2013**, *113*, 5110–5148. [[CrossRef](#)] [[PubMed](#)]
9. Bünzli, J.C.G.; Piguet, C. Lanthanide-containing molecular and supramolecular polymetallic functional assemblies. *Chem. Rev.* **2002**, *102*, 1897–1928. [[CrossRef](#)] [[PubMed](#)]
10. Li, X.Z.; Zhou, L.P.; Yan, L.L.; Dong, Y.M.; Bai, Z.L.; Sun, X.Q.; Diwu, J.; Wang, S.; Bünzli, J.C.; Sun, Q.F. A supramolecular lanthanide separation approach based on multivalent cooperative enhancement of metal ion selectivity. *Nat. Commun.* **2018**, *9*, 547. [[CrossRef](#)]
11. Lewis, F.W.; Harwood, L.M.; Hudson, M.J.; Drew, M.G.B.; Desreux, J.F.; Vidick, G.; Bouslimani, N.; Modolo, G.; Wilden, A.; Sypula, M.; et al. Highly efficient separation of actinides from lanthanides by a phenanthroline-derived bis-triazine ligand. *J. Am. Chem. Soc.* **2011**, *133*, 13093–13102. [[CrossRef](#)]
12. Montgomery, C.P.; Murray, B.S.; New, E.J.; Pal, R.; Parker, D. Cell-penetrating metal complex optical probes: Targeted and responsive systems based on lanthanide luminescence. *Acc. Chem. Res.* **2009**, *42*, 925–937. [[CrossRef](#)] [[PubMed](#)]
13. Charbonnière, L.J.; Ziessel, R.; Montalti, M.; Prodi, L.; Zaccheroni, N.; Boehme, C.; Wipff, G. Luminescent lanthanide complexes of a bis-bipyridine-phosphine-oxide ligand as tools for anion detection. *J. Am. Chem. Soc.* **2002**, *124*, 7779–7788. [[CrossRef](#)]
14. Wei, C.; Ma, L.; Wei, H.; Liu, Z.; Bian, Z.; Huang, C. Advances in luminescent lanthanide complexes and applications. *Sci. China Technol. Sci.* **2018**, *61*, 1265–1285. [[CrossRef](#)]
15. Klink, S.I.; Grave, L.; Reinhoudt, D.N.; Van Veggel, F.C.J.M.; Werts, M.H.V.; Geurts, F.A.J.; Hofstraat, J.W. A systematic study of the photophysical processes in polydentate triphenylene-functionalized Eu³⁺, Tb³⁺, Nd³⁺, Yb³⁺, and Er³⁺ complexes. *J. Phys. Chem. A* **2000**, *104*, 5457–5468. [[CrossRef](#)]
16. Chow, C.Y.; Eliseeva, S.V.; Trivedi, E.R.; Nguyen, T.N.; Kampf, J.W.; Petoud, S.; Pecoraro, V.L. Ga³⁺/Ln³⁺ Metallacrowns: A promising family of highly luminescent lanthanide complexes that covers visible and near-infrared domains. *J. Am. Chem. Soc.* **2016**, *138*, 5100–5109. [[CrossRef](#)]
17. Barry, D.E.; Kitchen, J.A.; Merces, L.; Peacock, R.D.; Albrecht, M.; Gunnlaugsson, T. Chiral luminescent lanthanide complexes possessing strong (samarium, Sm III) circularly polarised luminescence (CPL), and their self-assembly into Langmuir–Blodgett films. *Dalton Trans.* **2019**, *48*, 11317–11325. [[CrossRef](#)]
18. Walton, J.W.; Bari, L.D.; Parker, D.; Pescitelli, G.; Puschmann, H.; Yufit, D.S. Structure, resolution and chiroptical analysis of stable lanthanide complexes of a pyridylphenylphosphinate triazacyclononane ligand. *Chem. Commun.* **2011**, *47*, 12289–12291. [[CrossRef](#)]
19. Rinehart, J.D.; Long, J.R. Exploiting single-ion anisotropy in the design of f-element single-molecule magnets. *Chem. Sci.* **2011**, *2*, 2078. [[CrossRef](#)]
20. Li, X.Z.; Zhou, L.P.; Yan, L.L.; Yuan, D.Q.; Lin, C.S.; Sun, Q.F. Evolution of luminescent supramolecular lanthanide M₂nL₃n complexes from helicates and tetrahedra to cubes. *J. Am. Chem. Soc.* **2017**, *139*, 8237–8244. [[CrossRef](#)]
21. Bozoklu, G.; Gateau, C.; Imbert, D.; Pécaut, J.; Robeyns, K.; Filinchuk, Y.; Memon, F.; Muller, G.; Mazzanti, M. Metal-controlled diastereoselective self-assembly and circularly polarized luminescence of a chiral heptanuclear europium wheel. *J. Am. Chem. Soc.* **2012**, *134*, 8372–8375. [[CrossRef](#)]
22. Lama, M.; Mamula, O.; Kottas, G.S.; Rizzo, F.; De Cola, L.; Nakamura, A.; Kuroda, R.; Stoeckli-Evans, H. Lanthanide class of a trinuclear enantiopure helical architecture containing chiral ligands: Synthesis, structure, and properties. *Chem. Eur. J.* **2007**, *13*, 7358–7373. [[CrossRef](#)]
23. Mamula, O.; Lama, M.; Telfer, S.G.; Nakamura, A.; Kuroda, R.; Stoeckli-Evans, H.; Scopelitti, R. A Trinuclear EuIII Array within a diastereoselectively self-assembled helix formed by chiral bipyridine-carboxylate ligands. *Angew. Chem. Int. Ed.* **2005**, *44*, 2527–2531. [[CrossRef](#)]
24. Lama, M.; Mamula, O.; Kottas, G.S.; De Cola, L.; Stoeckli-Evans, H.; Shova, S. Enantiopure, supramolecular helices containing three-dimensional tetranuclear Lanthanide (III) arrays: Synthesis, structure, properties, and solvent-driven trinuclear/tetranuclear interconversion. *Inorg. Chem.* **2008**, *47*, 8000–8015. [[CrossRef](#)] [[PubMed](#)]
25. Dolomanov, O.V.; Bourhis, L.J.; Gildea, R.J.; Howard, J.A.K.; Puschmann, H. OLEX2: A complete structure solution, refinement and analysis program. *J. Appl. Cryst.* **2009**, *42*, 339–341. [[CrossRef](#)]
26. Sheldrick, G.M. SHELXT—Integrated space-group and crystal-structure determination. *Acta Cryst. A* **2015**, *71*, 3–8. [[CrossRef](#)] [[PubMed](#)]
27. Sheldrick, G.M. Crystal structure refinement with SHELXL. *Acta Cryst. C* **2015**, *71*, 3–8. [[CrossRef](#)]
28. Desreux, J.F. *Lanthanide Probes in Life, Chemical and Earth Sciences. Theory and Practice*; Bünzli, J.-C.G., Choppin, G.R., Eds.; Elsevier Science: Amsterdam, The Netherlands, 1989.

29. Lötscher, D.; Rupprecht, S.; Collomb, P.; Belser, P.; Viebrock, H.; Von Zelewsky, A.; Burger, P. Stereoselective synthesis of chiral pinene [5,6] bipyridine ligands and their coordination chemistry. *Inorg. Chem.* **2001**, *40*, 5675–5681. [[CrossRef](#)] [[PubMed](#)]
30. Steiner, T. The hydrogen bond in the solid state. *Angew. Chem. Int. Ed.* **2002**, *41*, 49–76. [[CrossRef](#)]
31. Lama, M.A. *Enantiopure Helical (Supra) Molecular Arrays Containing Lanthanides: Design, Synthesis and Properties*; EPFL: Lausanne, Switzerland, 2006; pp. Nr. 3708.
32. Mamula, O.; Lama, M.; Stoeckli-Evans, H.; Shova, S. Switchable chiral architectures containing PrIII Ions: An example of solvent-induced adaptive behavior. *Angew. Chem. Int. Ed.* **2006**, *45*, 4940–4944. [[CrossRef](#)]
33. Lewis, D.L.; Estes, E.D.; Hodgson, D.J. The infrared spectra of coordinated perchlorates. *J. Cryst. Mol. Struct.* **1975**, *5*, 67–74. [[CrossRef](#)]
34. Socrates, G. *Infrared and Raman Characteristic Group Frequencies: Tables and Charts*, 3rd ed.; Wiley: Chichester, UK, 2001.
35. Deacon, G. Relationships between the carbon-oxygen stretching frequencies of carboxylate complexes and the type of carboxylate coordination. *Coord. Chem. Rev.* **1980**, *33*, 227–250. [[CrossRef](#)]
36. Nakamoto, K. Frontmatter. In *Infrared and Raman Spectra of Inorganic and Coordination Compounds*; Wiley Online Books; John Wiley & Sons, Inc.: Hoboken, NJ, USA, 2008; pp. 1–147.
37. Kirby, A.F.; Richardson, F.S. Detailed analysis of the optical absorption and emission spectra of Eu³⁺ in the trigonal (C₃) Eu (DBM)₃·H₂O system. *J. Phys. Chem.* **1983**, *87*, 2544–2556. [[CrossRef](#)]
38. Düggele, M.; Christen, T.; Von Zelewsky, A. Protonation behaviour of chiral tetradentate polypyridines derived from α -pinene. *Chem. Eur. J.* **2005**, *11*, 185–194. [[CrossRef](#)]
39. Dux, F. titrationFitter 2020. Available online: <https://ypyi.org/project/titrationFitter/> (accessed on 15 November 2020).
40. Comby, S.; Imbert, D.; Chauvin, A.S.; Bünzli, J.C.G.; Charbonnière, L.J.; Ziessel, R.F. Influence of anionic functions on the coordination and photophysical properties of lanthanide (III) complexes with tridentate bipyridines. *Inorg. Chem.* **2004**, *43*, 7369–7379. [[CrossRef](#)] [[PubMed](#)]
41. Souri, N.; Tian, P.; Lecointre, A.; Lemaire, Z.; Chafaa, S.; Strub, J.-M.; Cianferani, S.; Elhabiri, M.; Platas-Iglesias, C.; Charbonnière, L.J. Step by step assembly of polynuclear lanthanide complexes with a phosphonated bipyridine ligand. *Inorg. Chem.* **2016**, *55*, 12962–12974. [[CrossRef](#)] [[PubMed](#)]